An Experimental Investigation of Turbulent Transonic Viscous-Inviscid Interactions

IRWIN E. ALBER*
TRW Systems, Redondo Beach, Calif.

AND

JOHN W. BACON†
Northrop Aerophysics Laboratory, Hawthorne, Calif.

AND

BRUCE S. MASSON‡
Aerospace Corporation, El Segundo, Calif.

AND

DONALD J. COLLINS§
Jet Propulsion Laboratory, Pasadena, Calif.

Experimental details are presented of the turbulent transonic separated flow generated on the rear portion of a two-dimensional circular-arc model mounted on the floor of a transonic duct ($M_\infty \simeq 0.7$). Two interaction modes were studied and are characterized by their peak Mach numbers: case A, that of pressure-gradient induced separation ($M_p < 1.32$), and case B, that of shock-induced separation ($M_p > 1.32$). Separation criteria are determined for both modes which are based on the velocity field of the viscous layer at separation. The measured reverse-flow velocity profiles are shown to compare favorably with theoretical similarity solutions based on the turbulent energy equation, and are employed to construct a velocity and streamline map of the flowfield. Using an approximate inviscid streamline shape for the separated flow, a time dependent finite-difference solution has been obtained for the inviscid transonic pressure distribution which shows reasonable agreement with measured wall pressures throughout the entire field.

Nomenclature

c = chord; $c = 12$ in.
$\mathscr{H}$ = θ/δ^*; boundary-layer shape parameter
t = model thickness; $t = 1.0$ in.
u_τ = $[\tau_w/\rho_w]^{1/2}$; friction velocity
u^* = van Driest reduced velocity
$\tilde{X}$ = $2X/c$
$\tilde{Y}$ = $2Y/c$
$\beta_p = -\dfrac{\theta}{U_e}\dfrac{dU_e}{dx}$; pressure gradient parameter
$\beta_t = \dfrac{\delta_k^*}{\tau_w}\dfrac{dP}{dx}$; Clauser pressure gradient parameter
δ = boundary-layer thickness; $u/u_e = 0.99$
δ^* = boundary-layer displacement thickness
$\tilde{\pi}$ = Coles wake parameter
θ = boundary-layer momentum thickness

Subscripts

e = boundary-layer edge
p = peak value
R = reattachment value
w = wall
k = van Driest reduced parameters

Presented as Paper 71-565 at the AIAA 4th Fluid and Plasma Dynamics Conference, Palo Alto, Calif., June 21–23, 1971; submitted June 26, 1972; revision received October 30, 1972. The work presented in this paper was performed while the authors were associated with the Northrop Corporate Laboratories, Hawthorne, Calif. The authors wish to express their sincere gratitude to the Northrop Corporation for supporting this research.

Index categories: Subsonic and Transonic Flow; Jets, Wakes, and Viscous-Inviscid Interactions.

* Staff Engineer, Fluid Mechanics Laboratory. Member AIAA.
† Manager of Internal Aerodynamics Testing.
‡ Member of the Technical Staff.
§ Senior Scientist. Member AIAA.

I. Introduction

WITH the continuing development of highly loaded wings for use at transonic speeds, it becomes increasingly more difficult to predict pressure distributions on full-scale airfoil sections. This difficulty is the result of the significant transonic viscous-inviscid interactions between the turbulent boundary layer and the outer inviscid flow.

Two modes of turbulent separation occur. The pressure-gradient mode is generally initiated at the trailing edge of a transonic, moderately thick airfoil ($t/c < 15\%$), and moves forward with increasing angle of attack. This mode of separation corresponds to the usual subsonic airfoil trailing-edge separation; its onset is a strong function of the local boundary-layer Reynolds number and of the local pressure gradient. In contrast, the initiation of the transonic shock-wave mode of separation is generally considered to be independent of Reynolds number (but linked to the presence of a boundary layer) and to be governed primarily by a supersonic viscous-inviscid interaction, characterized by a peak Mach number, $M_p > 1.2$–1.4.

In an early paper, Liepmann[1] reported schlieren and wall static-pressure measurements which revealed significant differences between laminar and turbulent boundary layers separating in the shock-interaction mode. The boundary-layer and inviscid flowfield measurements of Ackeret et al.,[2] and of Seddon[3] indicate that a rapid rise in boundary-layer displacement thickness occurs at separation which in turn produces a

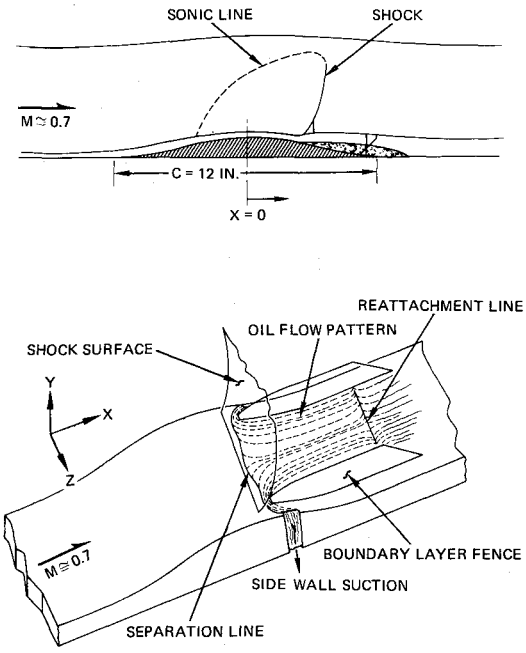

Fig. 1 Experimental setup and flowfield schematic.

significant modification of the wall pressure distribution from that which would be predicted from inviscid theory. Seddon also demonstrated the bifurcation of the incident normal shock wave into a strong oblique shock wave (generated by the viscous interaction) and a weak, nearly normal rear shock. The bifurcated, or lambda shock system is followed by a supersonic tongue which extends several boundary-layer thicknesses downstream of the shock wave in the region near the viscous layer edge. Seddon demonstrated that the final recompression in the tongue is isentropic.

In order to provide a quantitative description of these processes, the present experiments were undertaken to measure the detailed velocity and pressure fields associated with turbulent separation in both the shock-interation and the pressure-gradient separation modes. The static-pressure and total-pressure surveys described in Sec. II were used to determine the mean-velocity profiles both within the boundary layer, and in the adjacent inviscid flowfields (Sec. III and IV). These profiles are compared in Sec. IV with the theoretical reverse-flow profiles of Alber.[4] A comparison is made in Sec. V of measured wall pressures with those calculated by an inviscid time-dependent finite-difference method, using an approximation of the measured separated-flow streamline as a boundary condition.

II. Experimental Technique

The experiments were performed in a transonic duct at the Northrop Corporate Labs.¶ The duct, illustrated in Fig. 1, was a solid wall, continuous operating, indraft facility with a cross section of $3\frac{1}{2}$ by 9 in. The freestream Mach number was variable ($0.3 < M_\infty \leqq 0.8$), with a unit Reynolds number of $Re \approx 3 \times 10^5$/in. at $M_\infty \approx 0.7$. Water vapor condensation was prevented by maintaining a stagnation temperature of 585°R. Both boundary-layer suction and a variable area sonic throat downstream of the test section were used in order to stabilize the transonic pressure field. With this geometry, the flow was steady and the peak Mach number was reproducible to within $\pm 0.5\%$.

The model selected for these experiments differs from that used by Michel et al.[5] in that the present model was a modified circular-arc profile, 1.0 in. in height, which was smoothly faired into the floor at its extremities. The upper surface of the duct has been contoured to approximate a streamline of the unbounded inviscid flow, thus increasing the effective transonic tunnel parameter (cf., Fig. 1 and Ref. 6).

The aspect ratio of the separated flow (defined as the width of the tunnel divided by the length of the separated zone) was about 0.6 and was not sufficient to insure a two-dimensional flow. In order to alleviate the sidewall boundary-layer interaction, fences were installed in the vicinity of the sidewall boundary-layer edge, and sidewall suction was introduced near the leading edge of the fences (Fig. 1). Using these techniques, with verification by surface oil-flow visualization studies (Fig. 1) and by schlieren photography, it is felt that the flow throughout the interaction region was nearly spanwise uniform.

Detailed surveys have been made of both the impact-pressure and the static-pressure distributions using probes which enter the flow at discrete stations along the wall. The probes were oriented in the direction of the local mean flow and recorded the pressure by use of a Statham differential pressure transducer, referenced to stagnation conditions. For each profile, care was exercised in selecting the geometry of the probe in order to minimize the disturbance to the flowfield. The boundary-layer type pitot probes were constructed with a frontal height of 0.008 in. and the static-pressure probes were a 0.050-in.-o.d. cone-cylinder design (see Fig. 5 for characteristic boundary-layer dimensions).

The velocity profiles were computed without correcting for the influence of the wall on the measured impact pressures very near the surface and by assuming that the total temperature variation was that appropriate to a recovery factor of 0.885 at the wall. The resulting velocity profiles have been reduced to an equivalent incompressible form by using the compressibility transformation of van Driest.[7] In their reduced form, the profiles are least-squares fitted to the law of the wall and law of the wake at each station. It must be noted here that the difficulty of accurately determining the reversed-flow velocities in the separated-flow region, caused by the small differences between the measured pitot and static pressures, and enhanced for transonic flow by probe interference effects, implies that velocity ratios less than 0.05 cannot be determined reliably.

III. Wall Static-Pressure Results

At low subsonic Mach numbers ($M_\infty < 0.4$) the pressure distribution generally agrees with the classical linearized solution,[8] modified for compressibility by the Prandtl-Glauert correction, and computed for a body that closely resembles the model shown in Fig. 1. For $M_\infty = 0.35$, the experimental pressure distribution shown in Fig. 2 is nearly symmetric about the model centerline as predicted by linearized theory. However, the downstream pressure does not reach the maximum obtained upstream ($p/p_0 = 0.942$) because of the presence of a small separation bubble initiated at the point $\tilde{X} = 0.7$.

As the Mach number is increased, the symmetry which occurs at low speeds is lost as a consequence of the influence of both compressibility and separation (cf. Fig. 2). The locations of the separation and reattachment points (determined from oil flow observations) are shown in Fig. 3 as a function of peak Mach number M_p. For $M_p < 1.32$ the separation point moves upstream with increasing peak Mach number, and the reattachment point moves downstream. When the freestream Mach number exceeds $M_\infty = 0.65$, the flow is supercritical and Fig. 3 indicates the existence of a shock wave just downstream of the top of the model. For $M_p < 1.32$, the boundary layer does not separate at the shock (cf. Figs. 2 and 3) but separates at a point downstream in a region of further rising pressure.

An increase of the peak Mach number to 1.34 causes the separation point to move from its downstream location (marked A in Fig. 3; $\tilde{X} = 0.42$) to a position immediately aft of the foot of the shock (marked B in Fig. 3; $\tilde{X} = 0.23$). This effect is caused by a fundamental change in the mechanism which generates the

¶ The authors wish to acknowledge the assistance of L. Gross in the preliminary wind-tunnel measurements.

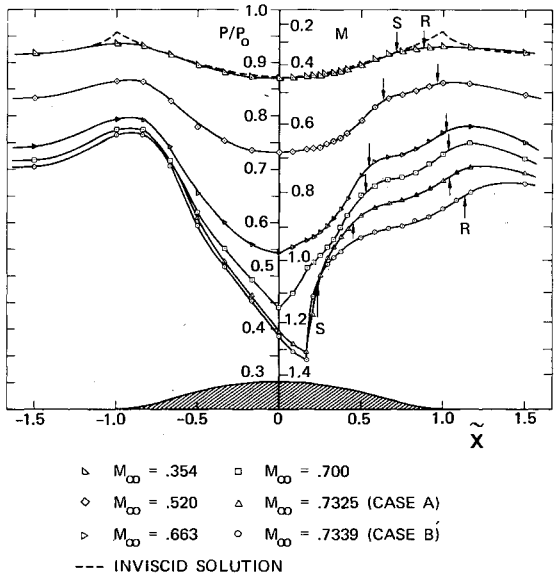

Fig. 2 Distribution of surface pressure.

separation bubble; that is, a change from pressure-gradient induced separation to shock-wave induced separation. The principal consequence is that the wall pressures in the region downstream of the shock wave are significantly reduced as shown in Fig. 4, while the pressure jump across the shock ($p_2/p_1 \sim 1.45$) remains unchanged. The value of M_p at which separation is initiated at the shock ($M_p \approx 1.32$) agrees with previous empirical correlations of the peak Mach number required for shock-wave induced separation. As the peak Mach number is increased beyond 1.34, the shock and the separation and reattachment points move downstream as shown in Fig. 3.

The geometry of the separation bubble is sensitive to small perturbations in the upstream pressure distribution, as shown by the results in Fig. 2. The separated flow generates a large effective afterbody which couples with the inviscid flow to determine the over-all flowfield by a strong interaction process. By measuring the velocity profiles in the separated region, it is possible to determine the displacement bodies (δ^*) for both flows, and hence the respective changes in the boundary conditions for the corresponding outer inviscid flows.

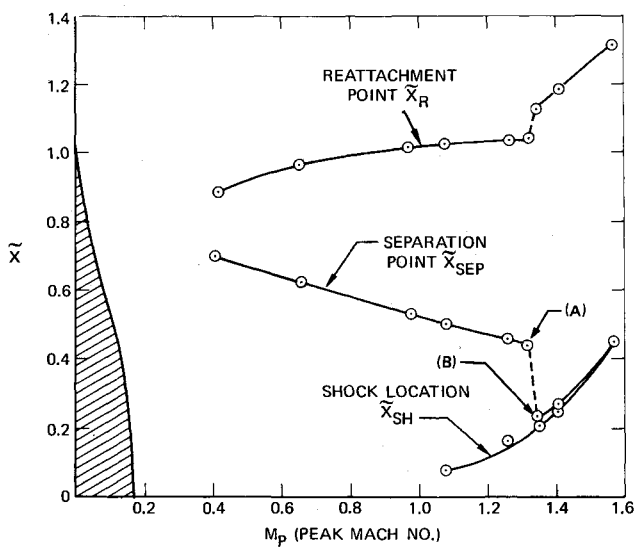

Fig. 3 Separation, reattachment and shock wave locations.

IV. Boundary-Layer Velocity Profiles

Comprehensive pitot and static-pressure surveys through the turbulent boundary layer were made for the two basic flows; case A, the pressure-gradient separation case ($M_p = 1.31$), and case B, the shock-separation case ($M_p = 1.34$). An indirect check of the two-dimensionality of the mean boundary-layer flow data has been obtained by evaluating, from the measured profiles, the appropriate terms in the two-dimensional momentum equation, in the manner suggested by Coles and Hirst.[9] The results of this evaluation (cf. Ref. 6) indicate that the flowfield can be considered to be reasonably two-dimensional for all of the data presented.

The velocity profiles upstream of the shock are nearly identical for both cases A and B. In the upstream pressure rise region, $-1.5 < \tilde{X} < -1.0$, the Clauser pressure gradient parameter $\beta_T = \delta_k^*(dp/dx)/\tau_w \approx 1.0$,** and the profiles at $\tilde{X} = -1.0$, -0.82 display characteristics typical of moderate pressure gradient turbulent boundary layers ($\tilde{\pi} \approx 1.8$ from the Coles fit). For $\tilde{X} > -0.8$, the strong negative pressure gradient ($\beta_T < -1.0$) causes the velocities near the wall to increase rapidly such that at $\tilde{X} = -0.33$, for example, $u/u_e \approx 0.90$ at a height above the wall of only 0.05δ. The outer 90% of the profile appears as a remnant of the upstream layer. As a result of the filling out of the inner portion of the profile, δ^* drops by nearly a factor of 4 during the upstream expansion process. This is shown in Fig. 5 where the integral properties δ^*, θ and $\mathscr{H} = \theta/\delta^*$, and the skin-friction coefficient C_f are presented as a function of distance $\tilde{X}$ for both cases. The profiles continue to exhibit an accelerated-flow character until the leading stem of the lambda shock is encountered ($\tilde{X} = 0.21$) just aft of the crest of the model (see

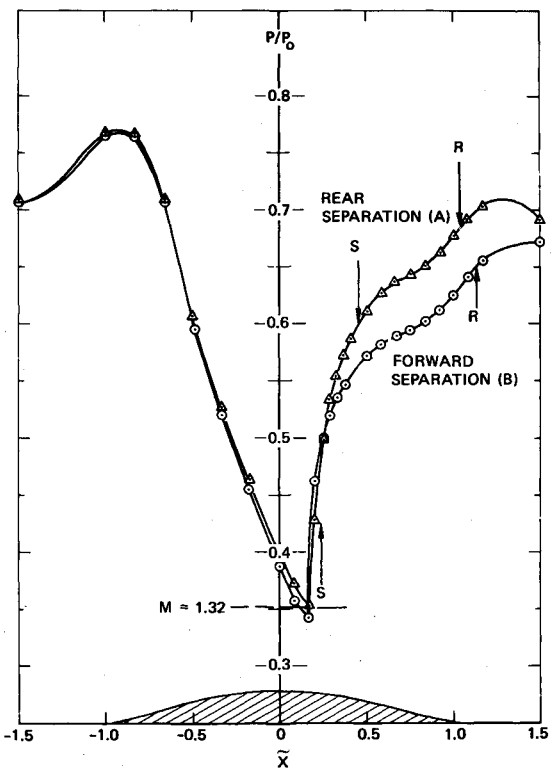

Fig. 4 Distribution of surface pressures for case A and B flows.

** When

$$\delta_k^* = \int_0^\delta (1 - u/u_e)\,dy$$

is used as a scale length for β_T, both compressible as well as incompressible pressure-gradient flows appear to show a similar velocity-profile wake behavior.[10]

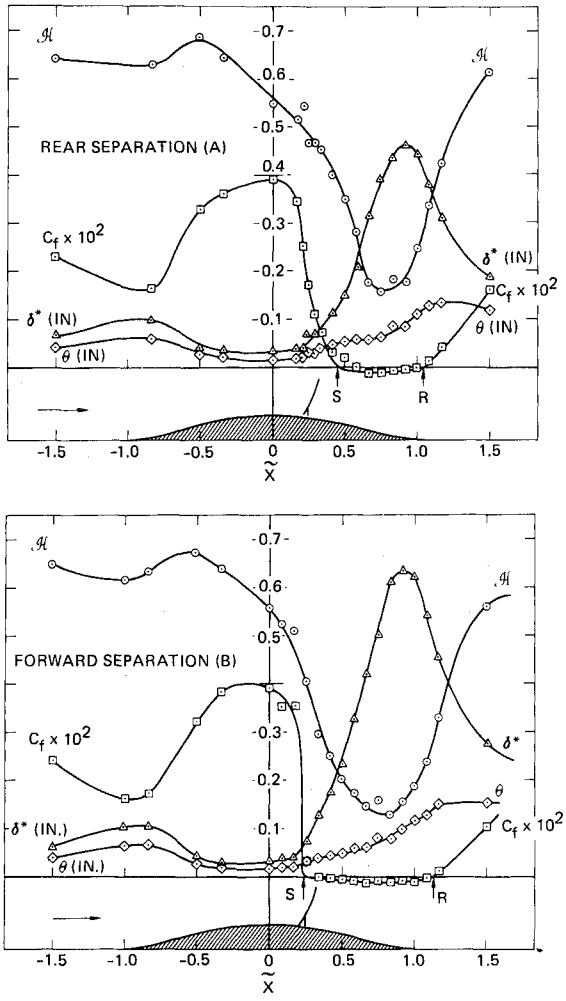

Fig. 5 Boundary-layer integral and wall shear distributions.

Fig. 5). Just downstream of this point, the velocity profile displays an interesting two region behavior shown in Fig. 6. For $y < 0.2$ in. the inner portion of the profile resembles a large β_T profile for case A and a slightly more restrained near-separation profile for case B. The outer portion of the profile ($y > 0.2$ in.) displays a further increase in velocity extending to a height of 0.5 in. This increased velocity results because the pitot and static probes have pierced the leading foot of the lambda shock and consequently encounter the higher velocity field above and ahead of the shock surface. Downstream, the velocity profiles and the boundary-layer growth begin to differ significantly for the two cases. In case A, the adverse pressure gradients initiated by the shock do not produce separation but cause the velocities near the wall to decrease, the boundary layer to grow rapidly ($d\delta^*/dx \approx 0.056$, about 20 times that of a flat-plate boundary layer), and the wall friction coefficient C_f to drop from a value of 3.6×10^{-3} to 0.7×10^{-3} at $\tilde{X} = 0.33$ (Fig. 5). In case B, where the shock-wave boundary-layer interaction is just strong enough to separate the flow near the shock, $d\delta^*/dx$ is larger, ≈ 0.10, C_f drops rapidly to zero just aft of the shock stem, and the profiles begin to develop a reverse-flow region near the wall (Fig. 6).

At $\tilde{X} = 0.45$, where the flow in case A separates because of the continuing adverse pressure gradient aft of the shock, the velocity develops a nearly linear profile (with an apparent slip velocity ratio of 0.1) having a shape factor $\mathcal{H} = 0.375$ ($\mathcal{H}_{\text{incomp}} \equiv \mathcal{H}_k \approx 0.429$). This separation profile is quite like the measured continuously separating incompressible profile of Stratford[11] ($\mathcal{H}_k = 0.429$) and the theoretical separation similarity solution of Alber.[4] Further comparisons between theory and data are presented in Sec. V.

Downstream of their respective separation points, both flows A and B develop large reverse velocities near the wall, giving the appearance of a negative wall jet. These reverse velocities reach a maximum negative value of $u/u_e = -0.15$ for case A and $u/u_e = -0.16$ for the larger separated flow of case B. These reverse-flow profiles have much the same character as the separated profiles recently measured by Behrens[12] in the recirculation region ahead of a forward facing step ($M_\infty = 4.0$), although his maximum reversed velocities were $(u_{\text{rev}}/u_e) \approx -0.37$. The height of the reverse velocity region, and the displacement of the outer flow, are greater for case B than for case A, because of the higher initial boundary-layer growth rate and the longer shock-induced separation bubble. This fact is evident in Fig. 5, where the maximum displacement thickness δ^* is shown to be 40% larger for case B than for case A.

In the outer part of the separated boundary layer, the velocity profiles develop from a wall-dominated flow near separation, to a wake or free shear-layer type flow near reattachment. A comparison of the experimental data in the outer region with the analytic representation of Coles' incompressible wake profile[13] (cf. Ref. 6),

$$u/u_e = \tfrac{1}{2}(1 - \cos \pi y/\delta) \equiv \tfrac{1}{2}\omega(y/\delta) \qquad (1)$$

indicates that the measured profiles appear to be approaching the limiting form given by Eq. (1). The rapid onset of reattachment, which occurs shortly aft of the downstream end of the model ($\tilde{X} > 1.0$) for both cases A and B, limits the further development of the outer profiles toward the form given by Eq. (1).

Downstream of reattachment, the profiles exhibit a strong wakelike character, with an increasing apparent slip velocity u_s near the wall (Fig. 6). These profiles are similar to those found in a wake flow following closure of a near-wake bubble. By $\tilde{X} = 1.5$, where longitudinal pressure gradients have diminished, the reattached profiles in both cases A and B are much thicker than their constant pressure counterparts upstream of the body ($\delta^*/\delta^*_{\tilde{X}=1.5} \approx 4$, case A). The downstream shape factors are 13% lower than the corresponding upstream values for case A, but the skin-friction coefficient at $\tilde{X} = 1.5$ is approximately half the value at the initial reference station. This indicates that the wall shear may be unimportant in the dynamics of the early reattachment period in the range $(x - x_R) \approx 5\delta$.

V. Modeling of the Transonic Separated Flowfield

A. Empirical Modeling

Using the velocity and pressure profiles discussed in Secs. III and IV, a complete picture of the important flowfield characteristics can be constructed, as shown in Fig. 6, where composite plots are presented of the streamlines and velocity profiles for case A and B flows. From the streamline plots of Fig. 6 it is evident that the streamline inclination deviates from the local wall slopes in the vicinity of separation. Further, the streamline deviations in case B are more pronounced than for case A since they are initiated further upstream at the shock wave and hence correspond to a thicker separation bubble. In case A, the streamlines show some deviation from the wall slope downstream of the shock, but the displacement effect does not become pronounced until the flow proceeds beyond separation. Since the two flows under investigation have nearly identical pressure distributions upstream of the shock, it is of interest to examine the mechanism which causes separation at the shock in case B but not in case A.

1. *Shock separation*

When the local Mach number at the edge of the boundary layer is supersonic, the nature of the interaction between the shock wave and the boundary layer depends primarily on whether the Mach number is greater than or less than some critical value.

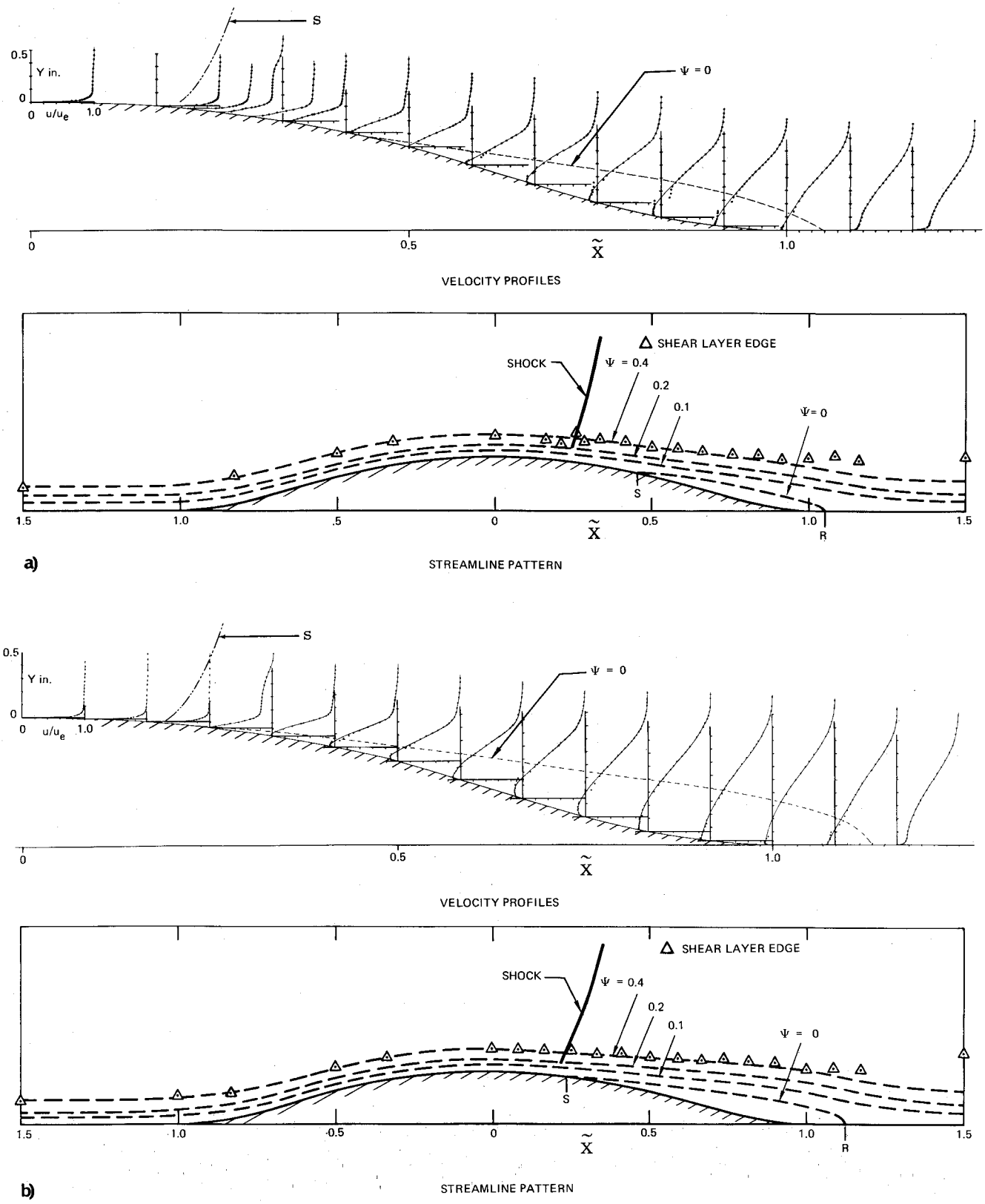

Fig. 6 Velocity profiles and streamline patterns for a) case A and b) case B flows.

The location of the shock wave depends to a great extent on the effective body shape, which is determined in part by the structure of the separation bubble (cf. Fig. 6). For the case of turbulent boundary-layer separation at the shock, most observations indicate that the separation process may be described by a free interaction which couples local pressure changes to the local turning angle through the Prandtl-Meyer relation, so long as the flow remains supersonic. The compression waves generated by the supersonic turning coalesce to form the leading foot of the lambda shock. Provided that separation has not occurred, so as to alter the local wall shape and velocity field, the maximum pressure ratio p_2/p_1, obtained by compressing isen-

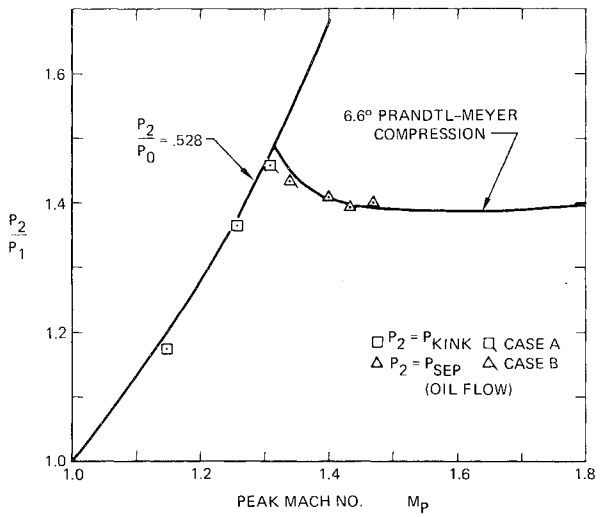

Fig. 7 Separation pressure rise criteria.

tropically to sonic speed, is limited by the magnitude of the local edge Mach number, and is plotted in Fig. 7 as a function of peak Mach number M_p.

An examination of the present data indicates that for $M_p < 1.32$, the regime for which separation occurs downstream of the shock wave, the compression proceeds smoothly up to and beyond the shock wave. Immediately downstream of the shock, a change occurs in the slope of the curve of wall pressure as a function of distance downstream. From these experiments (cf. Fig. 2), and from transonic data presented by other authors, e.g., Sinnott and Osborne,[14] the correlations indicate that this kink occurs near the sonic point in the flow and signals a change in the character of the flow from a supersonic to a subsonic interaction. This may be the analog of the supercritical-subcritical jump employed in theoretical treatments of separated flows (cf. Ref. 15). The pressure ratio for which the kink occurs has been plotted in Fig. 7 for peak Mach numbers less than 1.32.

In the second regime, typified by the case B streamline plots of Fig. 6, both the streamline near the boundary-layer edge ($\psi = 0.4$), and the measured δ^* contour experience a change in slope of approximately 6°in passing through the leading foot of the shock. For case B, the wall pressure rise to separation is 1.43, ($M_p = 1.34$) which corresponds to a Prandtl-Meyer angle change of 6.64° (Fig. 7). The difference in these angles may result from the normal pressure gradients produced by the wall curvature ($dp/dy > 0$). Hence the data indicate that separation cannot occur at the shock until the free-interaction compression turns the flow through approximately 6.6°. The lowest peak Mach number which can accomplish this before reaching sonic conditions is $M = 1.32$, the Mach number which divides case A, which separates downstream of the shock from case B, which separates in the shock interaction mode (Fig. 4).

If it is further hypothesized that the flow continues to separate at $\alpha = 6.6°$ for $M_p > 1.32$, then it is possible to calculate the pressure rise to separation, p_2/p_1, from the Prandtl-Meyer relation. This calculation is shown in Fig. 7 along with data for peak Mach numbers greater than 1.32, and the agreement is excellent. For peak Mach numbers between 1.4 and 2.0 the pressure rise remains nearly constant at a value of 1.4, which is consistent with a large number of transonic airfoil observations.[16] Seddon's[3] flat-plate separation data, at $M_p = 1.47$, indicate a value for α which is higher than that given by the present data by 1°.

2. *Pressure-gradient separation*

The peak Mach number for case A is just below that required to turn the flow through an angle $\alpha = 6.6°$ in the supersonic interaction mode. For this case, a possible low-speed pressure-gradient separation criteria has been discussed by Lees[17] and by Alber[4] which states that pressure-gradient separation is imminent if

$$\beta_p \equiv -\frac{\theta}{u_e}\frac{du_e}{dx} = \frac{\theta}{\rho_e u_e^2}\frac{dp}{dx} > 0.004 \tag{2}$$

This parameter is plotted in Fig. 8 as a function of position using the wall pressure and boundary-layer data of cases A and B to compute β_p. Near the shock location, β_p rises rapidly to a value greater than 0.007 for both cases A and B, with the case B flow separating in the supersonic shock-interaction mode near β_p max, as discussed in the preceding paragraph. Aft of the shock, β_p drops rapidly for both cases. However, for case A, β_p reaches a local minimum and then increases to a maximum value of 0.004. Slightly downstream of this local maximum the flow separates and β_p drops to a value of 0.001. Thus the case A flow does separate at a value of β_p close to the low speed criteria of 0.004, but only after first exceeding this value in the vicinity of the shock. In this case, the shock pressure rise is analogous to a supercritical-subcritical jump, which converts a profile that is supersonic on the average to a subcritical profile which allows disturbances to propagate upstream. In this framework the pressure gradients generated at the shock are felt instantaneously. Therefore, since the case A boundary layer did not separate in the supersonic interaction mode, the only gradients one need consider in determining the value of β_p for pressure-gradient separation are those downstream of the shock.

3. *Reattachment*

Five boundary-layer thicknesses downstream of the case A separation point (7δ for case B), the pressure gradients shown in Fig. 8 again increase, the shape factor $\mathscr{H}$ increases, and the separated flow approaches reattachment. At present there appears to be no definitive criteria for judging the length or pressure rise to reattachment of a transonic separation bubble. One clue to providing such criteria may lie in Fig. 8. It is noted that while the case A and B flows have separated by different criteria, they both reattach with nearly the same maximum value of $\beta_p \approx 0.0065$. By estimating the maximum reattachment pressure [by assuming $p_R = p_\infty$ or $p_R = p_{\max(x<x_{sep})}$] and the reattachment momentum thickness, θ_R, it is then possible to estimate the bubble length Δx_B from the equation,

$$\Delta x_B = \frac{\theta_R}{\gamma M_R^2}\frac{p_R - p_{sep}}{p_{sep}}\frac{1}{0.0065} \tag{3}$$

Initial calculations using measured values of θ_R, p_R and p_{sep} indicate fair agreement with the data.

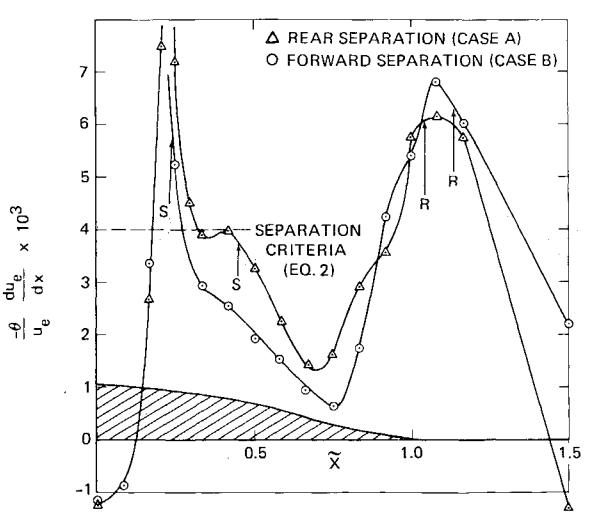

Fig. 8 Pressure gradient parameter distribution.

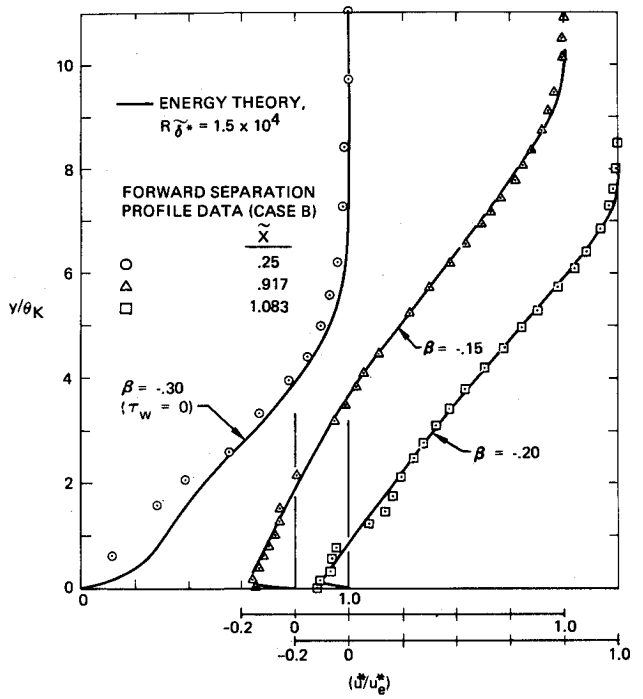

Fig. 9 Comparison of van Driest-reduced data with the theoretical turbulent energy similarity profiles of Alber.[4]

B. Theoretical Modeling

To develop a complete theoretical model for the transonic separation problem, calculations must be made of both the inner viscous and the outer inviscid flowfields, coupled as a strong interaction problem. In this section we will briefly discuss 1) the boundary-layer integral solutions upstream of separation, 2) the velocity profiles for the separated flow and reattachment regions, and 3) finite-difference solutions of the inviscid transonic flow with separationlike boundary conditions.

1. *Separated boundary-layer model*

Using the integral boundary-layer method of Alber and Coats[10] for compressible adiabatic boundary layers to calculate the appropriate initial conditions for the downstream shock-separation field, the flow can be modeled if a family of velocity profiles can be found which describes the turbulent boundary layer through the wide range of transonic pressure gradients and flow states, both attached and separated. In order to generate such a set of mean-velocity profiles, the present data were cast in the formulation of the law of the wall and the law of the wake in the manner suggested by Coles[9] for incompressible attached flows, extended to compressible adiabatic flows by employing the van Driest generalized velocities. A least-squares fit of the data was used to obtain the parameters of that formulation, δ, $f = u_\tau/u_e^*$ and $\tilde{\pi}$ (only 2 of which are independent if one employs the local friction law). The parameters are formally obtained in a manner similar to Mathews et al.[18] by minimizing the squared deviations of the reduced velocity data u^*/u_e^* given by

$$\frac{u^*}{u_e^*} = 1 + \frac{f}{\kappa}\left[\ln\frac{y}{\delta} - \tilde{\pi}\left(1+\cos\frac{\pi y}{\delta}\right)\right] \tag{4}$$

The comparison of the Coles least-squares fit with the measured velocity profiles (cf. Ref. 6) indicates that the Coles family gives an adequate representation of the velocity field both upstream and downstream of the separation point. However, the measured separation profiles do not correspond to Coles' zero wall-friction profile. It is further noted that the Coles family of profiles cannot aid directly in determining a model for the turbulent shear stresses in the vicinity of separation.

By extending the Mellor-Herring turbulent energy model to the case of turbulent separated flows, Alber[4] has demonstrated that the computed similarity solutions possess many of the important velocity profile properties exhibited, for example, by the continuously separating flow of Stratford[11] and by the mixing layer of Liepmann and Laufer.[19] Three typical separation velocity profiles, calculated from the incompressible similarity theory ($\beta = -0.3, -0.15, -0.2$), are shown in Fig. 9 and are compared with some of the case B, van Driest-reduced velocity data. The circled data on the left of Fig. 9 correspond to that portion of the velocity profile at $\tilde{X} = 0.25$ which lies below the shock, 0.1 in. downstream of the observed separation point. These data are compared with the theoretical zero shear ($\beta = 0.30$) separation similarity profile of Ref.4, plotted in the incompressible coordinates u^*/u_e^* vs y/θ_k. Some differences are noted near the wall, which are caused by the fact that the inner region of the measured profile is beginning to develop a post-separation character. The theoretical profiles chosen for comparison with the velocity profiles taken at $\tilde{X} = 0.917, 1.083$ were those profiles having approximately the same over-all shape factor $\mathscr{H}$. The agreement based on this simple one parameter identification of the profiles seems to be excellent.

To test the one parameter hypothesis further, all case A and B separated and attached data for the experimental (van Driest-reduced) mechanical energy shape factor $J_k = (\theta^*/\delta^*)_k$ and the mass flux shape factor $Z_k = [(\delta-\delta^*)/\delta^*]_k$ have been computed and are shown in Refs. 4 and 6.

2. *Inviscid outer flow model*

A time-dependent inviscid finite-difference code has been used to calculate the surface pressures (Fig. 10) and flowfield for the present transonic experiments in a manner similar to that used in Ref. 20. The code utilizes a rectangular mesh which extends one chord upstream and downstream of the model (60 mesh points), and extends across the tunnel (20 mesh points). Linearized boundary conditions are used such that the streamlines of the inviscid flow are tangent to the upper and lower boundaries. At the upstream boundary the total pressure is specified, while at the downstream boundary the conditions are set equal to those corresponding to the experiments.

The results of two numerical calculations are presented in Fig. 10. In the first calculation, shown as the dashed curve in

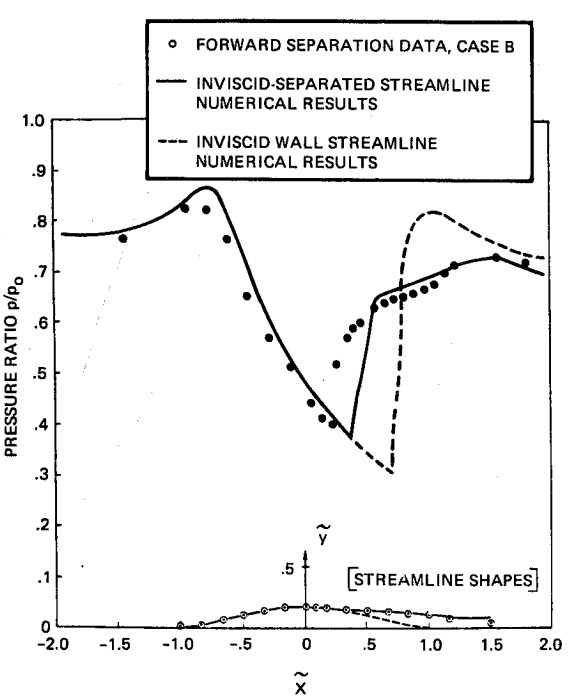

Fig. 10 Comparison of measured surface pressure distribution for case B with finite-difference solutions.

the figure, the upper and lower boundary conditions are computed from the geometry of the solid wall of the duct and from the model shape. In this case, the computed shock is both stronger and further downstream than indicated by the experimental data.

The second computation, shown by the solid curve in Fig. 10, was run in an attempt to model the effects of the viscous flow. In this case, the lower boundary, downstream of the measured shock-wave location, was approximated by a half-sine profile (cf. Ref. 6) in order to approximate the $\psi = 0.4$ streamline shape for the case B flow. The sine profile is joined to the model such that a 6° discontinuity occurs in the slope at the junction. The surface pressures computed using this inviscid separation streamline are in good agreement with the case B data (cf. Fig. 10). The shock location has moved upstream and is fixed by the compression corner. However, because of the coarse mesh, the shock does not bifurcate, and consequently the computed pressure rise across the shock is stronger than that observed experimentally.

VI. Conclusions

Detailed wall pressure and turbulent boundary-layer velocity profile data on a modified circular-arc model have been presented for two important cases of transonic shock-boundary layer interaction; that of pressure-gradient induced separation (case A), and that of shock-wave induced separation (case B). It was shown that for case A ($M_p < 1.32$), separation occurs downstream of the transonic shock at a point where the pressure gradient parameter

$$\beta_p = \theta(dp/dx)/\rho_e u_e^2 \approx 0.004$$

When the peak Mach number was raised to 1.34, the separation point jumped to the shock and the wall pressures in the post separation region dropped by about 10%. A criteria for the upstream peak Mach number just capable of producing shock-induced separation ($M_p \approx 1.32$) was deduced from the observed streamline angle change at the shock ($\alpha_{sep} \simeq 6.6°$) measured near the boundary-layer edge. It is argued that this angle fixes the pressure rise to separation at Mach numbers > 1.32. The value of β_p at reattachment was found to be nearly the same ($\beta_p \simeq 0.0065$) for both flows and may indicate a means for scaling separation bubble lengths.

Comparisons of measured separation and reverse-flow velocity profiles with the laws of the wall and wake indicate that this profile family can be extended to describe reverse-flow and reattachment profiles but cannot properly give the profile at the point $\tau_w = 0$. The separation profiles are well predicted by Alber's similarity solutions (including $\tau_w = 0$). It is thus surmised that the integral properties of these profiles can be adequately described by a one parameter representation.

Finally, it is demonstrated that numerical finite-difference solutions of the outer inviscid flow, when matched to an approximate separation streamline shape, give wall pressures for the separation region which show reasonable agreement with the data.

References

[1] Liepmann, H. W., "The Interaction Between Boundary Layer and Shock Waves in Transonic Flow," *Journal of the Aeronautical Sciences,* Vol. 13, No. 12, Dec. 1946, pp. 623–637.

[2] Ackeret, J., Feldmann, F., and Rott, N., "Investigation of Compression Shocks and Boundary Layers in Gases Moving at High Speed," TM 1113, Jan. 1947, NACA.

[3] Seddon, J., "The Flow Produced by Interaction of a Turbulent Boundary Layer with a Normal Shock Wave of Strength Sufficient to Cause Separation," R&M 3502, March 1967, Aeronautical Research Council, London, England.

[4] Alber, I. E., "Similar Solutions for a Family of Separated Turbulent Boundary Layers," AIAA Paper 71-203, New York, 1971.

[5] Michel, R., Marchaud, F., LeGallo, J., "Étude des Écoulements Trans-soniques Autour des Profiles Lenticulaires à Incidence Nulle," TP 65, 1953, ONERA, France.

[6] Alber, I. E., Bacon, J. W., Masson, B. S., Collins, D. J., "An Experimental Investigation of Turbulent Transonic Viscous-Inviscid Interactions," AIAA Paper 71-565, Palo Alto, Calif., 1971.

[7] Van Driest, E. R., "Turbulent Boundary Layer in Compressible Fluids," *Journal of the Aeronautical Sciences,* Vol. 18, No. 1, Jan. 1951, pp. 145–160.

[8] Allen, H. J., "General Theory of Airfoil Sections Having Arbitrary Shape or Pressure Distribution," TR 833, 1945, NACA.

[9] Coles, D. E. and Hirst, E. A., *Proceedings: Computation of Turbulent Boundary Layers—1968 AFOSR-IFP—Stanford Conference,* Vol. 2, Thermosciences Div., Dept. of Mechanical Engineering, Stanford Univ., Stanford, Calif., 1969.

[10] Alber, I. E. and Coats, D. E., "Analytical Investigations of Equilibrium and Nonequilibrium Compressible Turbulent Boundary Layers," AIAA Paper 69-689, San Francisco, Calif., 1969.

[11] Stratford, B. S., "An Experimental Flow with Zero Skin Friction Throughout its Region of Pressure Rise," *Journal of Fluid Mechanics,* Vol. 5, Pt. 1, 1959, pp. 17–35.

[12] Behrens, W., "Separation of a Supersonic Turbulent Boundary Layer by a Forward Facing Step," AIAA Paper 71-127, New York, 1971.

[13] Coles, D., "The Law of the Wake in the Turbulent Boundary Layer," *Journal of Fluid Mechanics,* Vol. 1, Pt. 2, July 1956, pp. 191–226.

[14] Sinnott, C. S. and Osborne, J., "Review and Extension of Transonic Aerofoil Theory," R&M 3156, Oct. 1958, Aeronautical Research Council, London, England.

[15] Lees, L. and Reeves, B. L., "Supersonic Separated and Reattaching Laminar Flows: I. General Theory and Application to Adiabatic Shock Wave Interactions," *AIAA Journal,* Vol. 2, No. 11, Nov. 1964, pp. 1907–1920.

[16] Pearcey, H. H., "Shock Induced Separation and its Prevention by Design and Boundary Layer Control," Pt IV, Vol. 2, *Boundary Layer and Flow Control,* edited by G. V. Lachmann, Pergamon Press, New York, 1961.

[17] Lees, L., "Turbulent Boundary Layer with Vanishing or Small Skin Friction," SAMSO TR 70-97, 1970, TRW Systems Group, Redondo Beach, Calif.

[18] Mathews, D. C., Childs, M. E., and Paynter, G. C., "Use of Coles' Universal Wake Function for Compressible Turbulent Boundary Layers," *Journal of Aircraft,* Vol. 7, No. 2, March 1970, pp. 137–140.

[19] Liepmann, H. W. and Laufer, J., "Investigations of Free Turbulent Mixing," TN 1257, 1947, NACA.

[20] Masson, B. S., Taylor, T. D., and Foster, R. M., "Application of Godunov's Method to Blunt Body Calculations," *AIAA Journal,* Vol. 7, No. 4, April 1969, pp. 694–698.